Additive Manufacturing Letters 2 (2022) 100032

Contents lists available at ScienceDirect

Additive Manufacturing Letters

journal homepage: www.elsevier.com/locate/addlet

Micro wire and arc additive manufacturing (μ-WAAM)

J.P. Oliveira*, Francisco M. Gouveia, Telmo G. Santos*

UNIDEMI, Department of Mechanical and Industrial Engineering, NOVA School of Science and Technology, Universidade NOVA de Lisboa, Caparica 2829-516, Portugal

ARTICLE INFO

Keywords:
Wire and arc additive manufacturing
Micro additive manufacturing
Process scaling
ASTMA 228

ABSTRACT

In this work we explore the wire and arc additive manufacturing (WAAM) process scale limits by using a wire diameter of 250 μm and about 2 mm stickout. This WAAM variant, named μ-WAAM, aims at competing with laser powder bed fusion technology, by enabling the fabrication of smaller parts with significantly higher deposition rates. The main issues of descaling the WAAM process are discussed and an acceptable parameter window to fabricate thin walls is presented. Several depositions were successfully performed with ASTMA 228 steel using a wire feed speed ranging from 75 to 90 mm/s, travel speed from 7 to 10 mm/s, a current intensity of 16 A RMS and power of ≈ 35 W RMS.

Introduction

Some fusion-based additive manufacturing (AM) technologies are predominantly oriented to the development of miniaturized components [1]. For these, powder bed fusion methods using a laser or an electron beam as the heat source are often used, and these technologies are capable of creating complex shaped functional and/or structural parts [2]. However, although powder bed fusion AM technologies have several advantages, including the high geometrical accuracy, they also possess several drawbacks such as low deposition rates and significant material waste [3].

In opposition to powder bed additive manufacturing, wire-feed technologies are often used to create larger structural components. Here, the heat source can be in the form of a high power beam (laser or an electron beam [4]) or an electric arc [5]. When arc-based heat sources are used, significantly high deposition rates can be obtained. However, although this feature is of major importance for an industrial context, it comes at the expense of the deposition accuracy and reduced ability to fabricate component with small, intricate geometries. This is related to the heat source dimensions: while for laser and electron beam AM the heat source can be drastically reduced, the same is not true for arc-based AM, due to the relatively large wire diameter used ($ø > 1$ mm). For this reason, the high deposition rate associated to arc-based AM is always counterbalanced by low geometrical precision/accuracy.

The ability to combine key features of both arc and high-power beams AM could render a significant impact towards a more massive adoption of AM technologies by industry. For example, achieving deposition rates similar to those found in arc-based AM while maintaining the geometrical accuracy and resolution of laser and electron beam-based AM would be a major paradigm shift in the current state of the art of fusion-based additive manufacturing.

Arc-based additive manufacturing lay its foundations in traditional and well-established welding technologies [6]. The electrical arc is a physical phenomenon and therefore, different technologies can be developed around it. Conventional wire and arc additive manufacturing (WAAM) typically uses wire diameters of 1 mm or above [7–9], thus its resolution cannot be lower than this and in fact even achieving such resolution is a tortuous and often complex task. Since the electrical arc is a physical phenomenon [6,10], it may be possible to scale it down, by using appropriate technologies and means. However, scaling down the electrical arc for additive manufacturing is not only a matter of geometrical scale. It involves new scaling issues and limitations. For example, the power that is possible to transmit through the wire prevents the wire from melting when small diameters are used since the surface lateral area to volume ratio of the wire increases according to $4/ø$, where ø [m] is the wire diameter. Moreover, the energy needed to melt thin wires is significantly lower than when a conventional filler wire is used. This means that the thermal cycle is less abrupt and most likely the transfer heat towards the substrate and/or previously deposited layers may not be enough to promote their remelting and ensure sound joining between consecutively deposited layers [11].

Some attempts to reduce the scale during fusion-based additive manufacturing of metals have been pursued lately. For example, micro selective laser melting has been seeing a tremendous increase in terms of published research in recent years [12]. Moreover, Demir [13] has evidenced the ability to successfully create thin-walled structures using micro laser metal wire deposition. Similarly, micro plasma transferred arc AM was successfully used to deposit wires with a diameter of 300 μm [14–16]. So far, there are no reports on the use of a heat source based

* Corresponding authors.
E-mail addresses: jp.oliveira@fct.unl.pt (J.P. Oliveira), telmo.santos@fct.unl.pt (T.G. Santos).

https://doi.org/10.1016/j.addlet.2022.100032
Received 20 November 2021; Received in revised form 18 January 2022; Accepted 21 January 2022

Table 1
Comparison of the typical values for SLM [1], conventional WAAM [17] and μ-WAAM processes.

Process	Layer thickness(μm)	Deposition rate(g/min)	Surface quality*(mm)
SLM [1]	25–75	0.5–2	±0.04
WAAM [17]	~1500	50–130	±0.7
Micro WAAM (obtained values)	<600	1.5–5–0	<0.3

* Surface quality is calculated as (TWW - EWW) / 2, where TWW refers to the total wall width, and EWW refers to the effective wall width.

Table 2
Main issues derived from μ-WAAM.

Potential issue	WAAM situation	μ-WAAM situation	Consequence
Wire diameter	About 1 mm corresponding to a section area of 0.79 mm^2	About 0.25 mm (0.03 mm^2 area is 26 times smaller)	Maximum power through wire can prevent its melting; heat transfer to the substrate and/or previously deposited layer can prevent remelting; wire is prone to plastic instability
Torches	Conventional welding torches are used	Conventional welding torches cannot deal with sub 0.3 mm diameter wires	Customized torches must be developed to feed sub 0.5 mm diameter wires
Welding source	Conventional welding sources allow suitable I-V curves	Voltage and current intensity are too low to be provided by conventional welding sources	Alternative sources must be used to create and stabilize an electrical arc with small arc length
Transfer modes	Typical welding transfer modes apply to fusion welding	Unknown since the material deposition is yet to be evaluated	Gravity vs surface tension forces that aid or prevent a drop to detach may have a more prominent impact due to the small size of the wire and subsequently of the material deposited

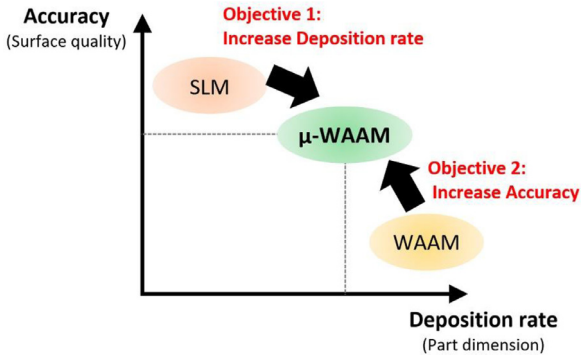

Fig. 1. Schematic illustration of the rational for using μ-WAAM when compared to selective laser melting (SLM) and conventional WAAM. The goals are to improve the deposition rate and the part accuracy simultaneously.

on metal inert gas (MIG) welding to create sub-millimeter deposits, only using plasma and tungsten inert gas (TIG) welding heat sources. The reason for such is related to process control: while in plasma and TIG-based processes the wire to be deposit does not influence the electric arc, the same does not apply to MIG/MAG processes. Here, the electric arc must be established between the wire feedstock material and the substrate, and its small diameter dimension and previously discussed limitations can prevent a stable arc to form and aid in the deposition of material.

In this work we showcase for the first time the μ-WAAM process based on a custom made MIG-based prototype. The rationale for developing this novel WAAM-based technology is to combine the advantages of both conventional WAAM and powder bed additive manufacturing, as detailed in both Table 1 and Fig. 1. Being this a preliminary study, some fundamental questions need to be answered, namely the following two: is it possible to transfer enough energy to the electric arc through small diameter wires (≈250 μm)? If so, is it possible to deposit several beads and guarantee a metallurgical bonding to the substrate and between layers?

μ-WAAM process specifications

As previously mentioned, scaling down the WAAM process implies some issues do not present in conventional WAAM where wire diameters of at least 1 mm are used. The main issues associated to the descaling of the WAAM process are detailed in Table 2.

Materials and methods

A customized WAAM torch was developed together with a small moving device (refer to Fig. 2). The moving device is a conventional XYZ linear table, with linear bearings, actuated by conventional step motors. The wire feed device was inspired by a conventional 3D material extrusion mechanism: one drive gear actuated by a step motor compressed under a radial bearing. Control of the μ-WAAM system axes is performed using the Repetier Software. To establish the electric contact with the wire, a 0.3 mm brass nozzle was used. A 12 V battery with 100 Ah capacity (VARTA Silver Dynamic H3) was used as the power source. The need to use a battery is related to the fact that conventional welding sources do not provide the adequate I-V characteristics for a such small welding arc. Different power electric resistances were connected in series with the electric arc allowing to change the arc voltage and the electric intensity. ASTM A228 wire with a diameter of 250 μm was used to deposit multiple layers with a length of roughly 10 mm in a mild steel substrate. The ASTM A228 wire has a carbon, manganese and silicon contents ranging from 0.7 to 1.0, 0.2 to 0.6 and 0.1 to 0.3 wt.%, respectively. For the single wall deposited samples, a one-way deposition strategy was adopted wherein the torch always returned to the same starting point. The arc voltage and the electric current were both measured using a sample rate of about 27 k samples/second with a current transducer LEM HTA 600-S and a 14-bit ADC converter Digilent Analog Discovery 2, according to the procedure described in [18]. A high-speed camera (Photron Mini WX50) was used to acquire videos of the μ-WAAM tests at 5000 fps with 768 × 512 image resolution. Slow motion color videos where also acquired at 960 fps with 1280 × 720 image resolution. Acoustic pressure was acquired with a microphone with 32-bit/384 kHz. Different μ-WAAM process parameters were tested to establish the adequate working conditions (refer to Table 3). The shielding gas used in this work (refer to Table 3) was selected to avoid process-induced defects such as pores, and to protect the material against oxidation due to the high temperatures that occur locally during deposition.

Results and discussion

Several μ-WAAM deposition tests were performed to determine suitable operating conditions. For different combinations of travel and wire

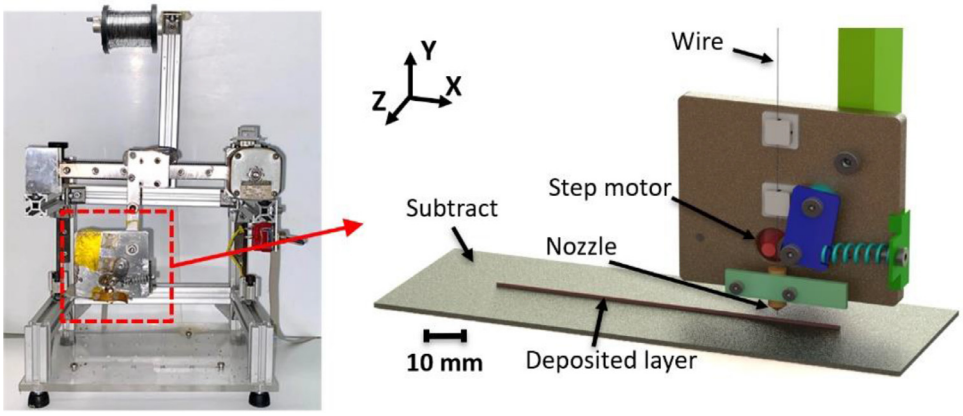

Fig. 2. Customized moving device and schematic representation of the μ-WAAM torch depositing one layer. A video of the system operating is available as supplementary material (temporarily here: Folder).

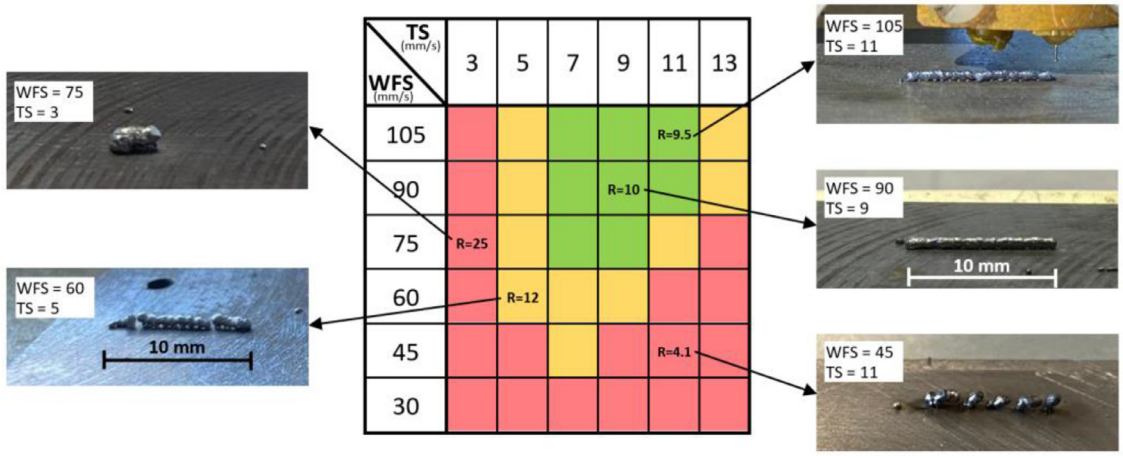

Fig. 3. Admissible combination of Wire Feed Speed (WFS) and Travel Speed (TS) for μ-WAAM using a ASTM A228 wire with 250 μm diameter.

Table 3
Process parameters used during μ-WAAM.

Welding mode	Gas metal arc welding – continuous mode (DC+)
Number of layers	1 or 10
Wire feed speed (WFS)	from 30 to 105 mm/sec (optimum: 75–90 mm/sec)
Travel speed (TS)	from 3 to 13 mm/sec (optimum: 6–9 mm/sec)
Voltage (during short circuit)	from 1 to 3 V (depending on electric resistances)
Electric current	from 10 to 20 A RMS (optimum: ≈16 A RMS)
Contact tip to work distance	2 mm
Shielding gas	ARCAL™ 121 (81%Ar + 1% CO_2 + 18% He)
Gas flow rate	10 L/min

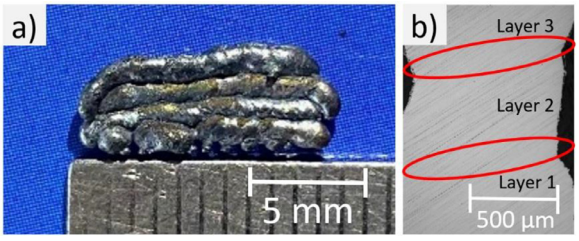

Fig. 4. One-way deposition single wall samples produced by μ-WAAM using ASTM A228 wire with 250 μm diameter. (a) four layers wall, (c) transversal section of (b) showing sound adhesion between layers.

feed speeds distinct geometrical attributes were obtained as detailed in Fig. 3. From this assessment it was decided to create single walls using the process parameters comprising a wire feed speed of 90 mm/s and a travel speed of 9 mm/s. The red and yellow colors detailed in Fig. 3, corresponded to single deposits that did not present a continuous deposition of material or when that happened the adherence to the substrate was poor or even non-existent.

A sound joint between adjacent layers was obtained (refer to Fig. 4) for the viable process conditions, highlighting the potential of μ-WAAM to create small-sized parts of relevant engineering materials.

The current and voltage waveforms captured during the process are depicted in Fig. 5. The waveform resembles a short circuit transfer mode [19] and the average time between consecutive short circuits was measured to be ≈12.5 ms. Of special relevance in these current and voltage waveforms is the associated power. While the power root mean square (RMS) was of 34.9 W, there are minor time frames (when short circuit occur) upon which the power reaches up to 200 W. This significant increase in the available power for melting and deposit the wire can modify the transfer mode temporarily, meaning that a combination of short circuit and most likely globular transfer occur. While there are other transfer modes available, it is considered that the prescribed values of current and voltage are not enough to allow for the spray transfer mode to be activated.

A close-up to the waveform for both current and voltage corresponding to one full cycle is depicted in Fig. 6. The short circuit spans for over ≈4.5 ms, while the open circuit is roughly 8 ms. Four distinct regions are marked in Fig. 6 which correspond to different process conditions as captured during by the high-speed imaging detailed in Fig. 7. Point 1 corresponds to the onset of the short circuit (voltage decrease and current increase until almost 48 A), which proceed until point 2. During this period the Joule effect is predominant. At point 3, end of the short

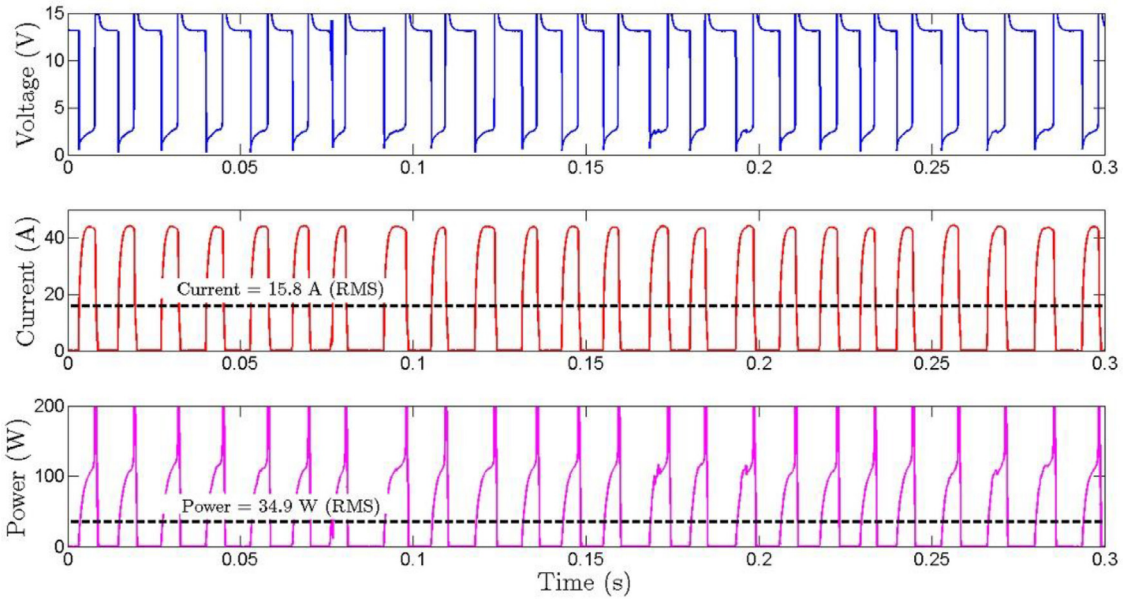

Fig. 5. Typical evolution of voltage and current intensity along time during μ-WAAM of ASTM A228 wire with 250 μm diameter with wire feed speed (WFS) of 75 mm/s and a travel speed (TS) of 6 mm/s. The root mean square (RMS) of the current is 15.8 A and the RMS power is 34.9 W. The average time between consecutive current peaks is about 12.5 ms, corresponding to a frequency of about 80 Hz. The raw data is available as supplementary material (temporarily here: Folder).

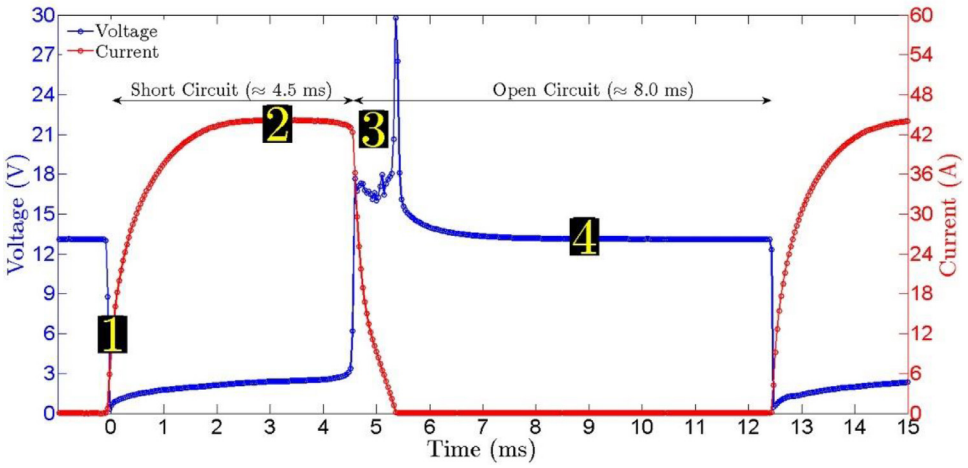

Fig. 6. Detailed evolution of voltage and current intensity along time during μ-WAAM of ASTM A228 wire with 250 μm diameter with wire feed speed and travel speed of 75 and 6 mm/sec, respectively. Zones 1 to 4 corresponds to the frames depicted in Fig. 7. The raw data is available as supplementary material (temporarily here: Folder).

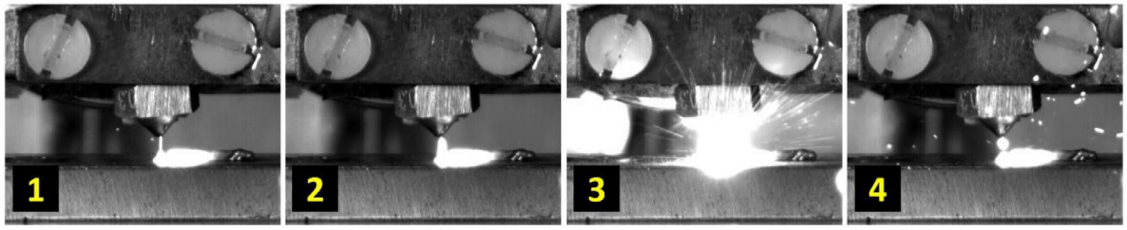

Fig. 7. Transfer mode during μ-WAAM of ASTM A228 wire with 250 μm diameter. The different instants correspond to the zones depicted in Fig. 6, namely, (1) beginning of short circuit; (2) Joule effect during short circuit; (3) explosion effect; (4) open circuit after explosion. The video at 5000 fps from where these images were obtained is available as supplementary material (temporarily here: Folder).

circuit occurs which was accompanied by an explosion of material, generating some spattering. After the end of the short circuit and explosion, the open circuit phase is established, and consequently, the voltage return to about 12 V (it exceeds slightly this value because the battery was new and was fully charged) and the current is 0 A.

Analysis of the sound pressure during the μ-WAAM process is shown in Fig. 8. The time between each peak is in good agreement with the process period (≈12.5 ms). After each major peak, which corresponds to the short circuit, there is a smooth decrease of the sound pressure that is attributed to the explosion of the material right after the short circuit phase. The low and almost constant sound pressure after the explosion occurs during the open circuit phase of the process.

Finally, Fig. 9 details the process evolution using a colorized frame. It can be seen that an electric arc (blueish color between time periods of

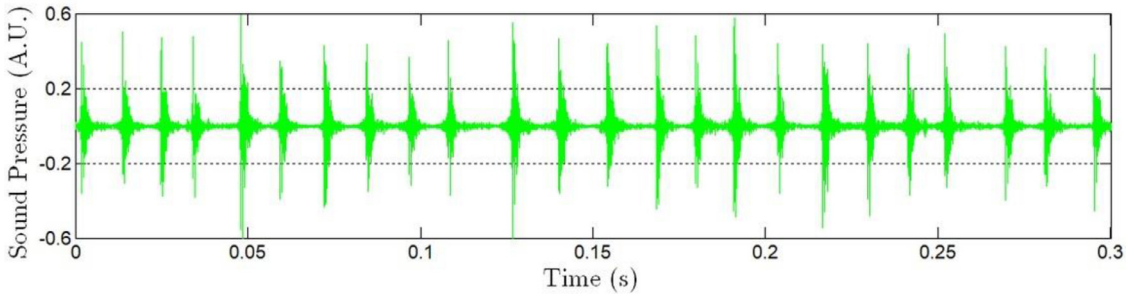

Fig. 8. Acoustic pressure acquired during μ-WAAM of ASTM A228 wire with 250 μm diameter. The peaks of the sound pressure correspond to the explosion effect (frame 3 of Fig. 7), and it agrees well with the period of the cycles (≈ 12.5 ms). The sound file is available as supplementary material (temporarily here: Folder).

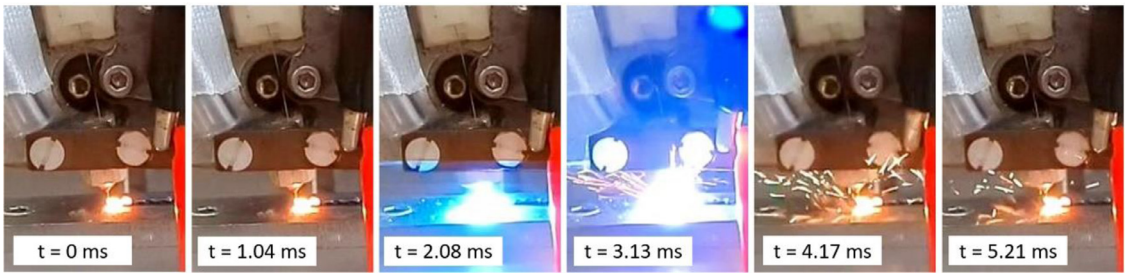

Fig. 9. Successive color frames acquired at 960 fps during μ-WAAM of ASTM A228 wire with 250 μm diameter. The frame n. 3 (t = 2.08 ms) shown the existence of an arc welding (plasma) for a short period of time followed by the explosion effect. The original video is available as supplementary material (temporarily here: Folder).

2.08 and 3.13 ms) is established momentarily, after a short circuit period with Joule effect (until the second frame). However, unlike typical arc-based processes, the time fraction at which the electrical arc is stable is rather small (about 1 ms). Future work will address in more detail the arc formation and stabilization during μ-WAAM since it is clear the need to understand the physics behind such a small electrical arc to obtain full process control during deposition. The explosion of material and spatter formation is seen to occur after the electric arc is interrupted.

The experimentally measured power of 34.9 W root mean square (RMS) is good agreement with the amount of thermodynamical power required to melt the deposited material deposited. According to the fundamental law of calorimetry (Eq. (1)) the theorical power is the product of the mass of the melted wire, m [kg], its specific heat capacity, C_p [J/kg °C] and the melting temperature, ΔT [°C], per unit of time, t [sec]. An additional amount of energy ΔE [J] should be considered regarding the compensation of the heat dissipation loss to the surrounding environment, the need to partially melt the substrate and/or previously deposited layer and the energy necessary for the phase transformation (fusion) due to the latent heat of the deposited material.

Eq. (2) is equivalent to Eq. (1), by substituting the mass by the product of the density, ρ [Kg/m^3], wire feed speed, [m/sec], and cross-sectional area, A [m^2]. Computing Eq. (2) (using 7800, 75, 520 and 1600 respectively for density, WFS, C_p and temperature) a value of 23.9 W is found, that is below the measured 34.9 W. The difference between the theorical value (23.9 W) and the measured one (34.9 W) can be ascertained to the fact that, for simplicity, we are ignoring the above-mentioned extra amount of power and we are limiting the maximum temperature reached to 1600 °C.

$$Power > \frac{m \cdot C_p \cdot \Delta T}{t} + \frac{\Delta E}{t} \quad (1)$$

$$Power > (\rho \cdot WFS \cdot A) \cdot C_p \cdot \Delta T + \frac{\Delta E}{t} \quad (2)$$

Finally, we compare some typically process features (such as power, volumetric energy and deposition rate) for both WAAM and μ-WAAM. For direct and reliable comparison, the authors of the present paper recorded these values from their own WAAM and μ-WAAM experiments. These values are detailed in Table 4. The major differences are on the available power necessary to deposit the wire, the wire feed speed and on the volumetric energy and deposition rate. The higher amount of power required in WAAM is related to two major effects: (i) need to melt (or remelt) a significant part of the substrate (or a previously deposited layer), which requires more energy; (ii) the longer distance between the tip of the wire to be deposit and the substrate requires that more heat is introduced to the material to compensate the heat losses during travelling upon droplet detachment. For μ-WAAM there is almost no melting of the substrate or previously deposited layers, and the distance between the tip of the wire and the substrate is below the millimeter scales, which prevents significant heat losses upon the detachment of the molten material.

Table 4
Comparison of key process parameters between μ-WAAM and WAAM [5,8,17].

Process parameters	WAAM	μ-WAAM
Wire diameter [mm]	1	0.25
Current [A]	120	15.8
Voltage [V]	20	2.2
Power [W]	2400	34.7
Travel speed [mm/s]	6	11
Wire feed speed [mm/s]	50	105
Heat input [J/mm]	400	5.2
Volumetric energy [J/mm^3]	61.1	6.7
Deposition rate [g/min of steel]	18.5	2.4

The higher wire feed speed required for μ-WAAM is related to the thermal conditions associated with the process. Since melting of the material is facilitated by its lower volume there is a need for a higher wire feed speed to allow its successful deposition. The later point also explains why the volumetric energy is significantly lower for μ-WAAM than for WAAM.

As for the deposition rate, although for μ-WAAM this is nearly seven times lower than conventional WAAM (due to the volume effects arising

from the larger diameter wires are used), the deposition rate associated with μ-WAAM is higher than that associated with powder bed additive manufacturing processes.

Conclusions

This paper presents an experimental validation of a new variant of WAAM, named μ-WAAM, by exploring the size limits of arc-based additive manufacturing. A customized μ-WAAM torch and a moving head were developed, manufactured, and tested. Single walls were fabricated using 250 μm ASTMA 228 wire. The ability to fabricate defect-free walls using this novel WAAM variant is relevant because conventional WAAM uses 1 mm (or above) diameter wires, thus limiting the process resolution to the wire diameter. The μ-WAAM variant significantly approaches the resolution of laser powder bed fusion additive manufacturing compared to conventional WAAM technology, while increasing the deposition rate. By further descaling the WAAM process to the micro level it is possible to preserve the high deposition characteristics of WAAM, with major improvements at the resolution level.

An electric arc is established within a small-time frame of ≈ 1 ms after which material explosion and spatter regeneration occurs. From the current and voltage waveforms a short circuit transfer mode occurs, with a total time of 4.5 ms in short circuit and 8 ms in open circuit. The process period, as determined by the current and voltage waveforms, is in good agreement with the acoustic pressure measurements. In these latter measurements, arc ignition and extinction as well as the material explosion are identified.

Future work will encompass further microstructure and mechanical characterization and evaluate how the process parameter window influence the deposition characteristics and geometrical features of the μ-WAAM deposited parts. More detailed understanding of the physics behind the generation of such small electrical arcs and how these impact the material transfer is currently being performed.

Declaration of Competing Interest

The authors declare that they have no known competing financial interests or personal relationships that could have appeared to influence the work reported in this paper.

Acknowledgments

Authors acknowledge the Portuguese Fundação para a Ciência e a Tecnologia (FCT - MCTES) for its financial support via the project UID/EMS/00667/2019 (UNIDEMI). This activity has received funding from the European Institute of Innovation and Technology (EIT) – Project Smart WAAM: Microstructural Engineering and Integrated Non-Destructive Testing. This body of the European Union receives support from the European Union's Horizon 2020 research and innovation program.

Supplementary materials

Supplementary material associated with this article can be found, in the online version, at doi:1016/j.addlet.2022.100032.

References

[1] T. DebRoy, H.L.L. Wei, J.S.S. Zuback, T. Mukherjee, J.W.W. Elmer, J.O.O. Milewski, A.M.M. Beese, A. Wilson-Heid, A. De, W. Zhang, Additive manufacturing of metallic components – Process, structure and properties, Prog. Mater. Sci. 92 (2018) 112–224, doi:10.1016/j.pmatsci.2017.10.001.

[2] M.M. Francois, A. Sun, W.E. King, N.J. Henson, D. Tourret, C.A. Bronkhorst, N.N. Carlson, C.K. Newman, T. Haut, J. Bakosi, J.W. Gibbs, V. Livescu, S.A. Vander Wiel, A.J. Clarke, M.W. Schraad, T. Blacker, H. Lim, T. Rodgers, S. Owen, F. Abdeljawad, J. Madison, A.T. Anderson, J.L. Fattebert, R.M. Ferencz, N.E. Hodge, S.A. Khairallah, O. Walton, Modeling of additive manufacturing processes for metals: challenges and opportunities, Curr. Opin. Solid State Mater. Sci. 21 (2017) 198–206, doi:10.1016/j.cossms.2016.12.001.

[3] J.P. Oliveira, A.D. LaLonde, J. Ma, Processing parameters in laser powder bed fusion metal additive manufacturing, Mater. Des. 193 (2020) 1–12, doi:10.1016/j.matdes.2020.108762.

[4] L. Murr, S. Gaytan, D. Ramirez, Metal fabrication by additive manufacturing using laser and electron beam melting technologies, Mater. Sci. Technol. 28 (2012) 1–14, doi:10.1016/S1005-0302(12)60016-4.

[5] B. Wu, Z. Pan, D. Ding, D. Cuiuri, H. Li, J. Xu, J. Norrish, A review of the wire arc additive manufacturing of metals: properties, defects and quality improvement, J. Manuf. Process. 35 (2018) 127–139, doi:10.1016/j.jmapro.2018.08.001.

[6] J.P. Oliveira, T.G. Santos, R.M. Miranda, Revisiting fundamental welding concepts to improve additive manufacturing: from theory to practice, Prog. Mater. Sci. 107 (2019) 100590, doi:10.1016/j.pmatsci.2019.100590.

[7] K. Oyama, S. Diplas, M. M'hamdi, A.E. Gunnæs, A.S. Azar, Heat source management in wire-arc additive manufacturing process for Al-Mg and Al-Si alloys, Addit. Manuf. 26 (2019) 180–192, doi:10.1016/j.addma.2019.01.007.

[8] C.R. Cunningham, J.M. Flynn, A. Shokrani, V. Dhokia, S.T. Newman, Invited review article: strategies and processes for high quality wire arc additive manufacturing, Addit. Manuf. 22 (2018) 672–686, doi:10.1016/j.addma.2018.06.020.

[9] J. Wang, Z. Pan, L. Wei, S. He, D. Cuiuri, H. Li, Introduction of ternary alloying element in wire arc additive manufacturing of titanium aluminide intermetallic, Addit. Manuf. 27 (2019) 236–245, doi:10.1016/j.addma.2019.03.014.

[10] D. Iordachescu, L. Quintino, R. Miranda, G. Pimenta, Influence of shielding gases and process parameters on metal transfer and bead shape in MIG brazed joints of the thin zinc coated steel plates, Mater. Des. 27 (2006) 381–390, doi:10.1016/j.matdes.2004.11.010.

[11] S. Mereddy, M.J. Bermingham, D.H. St John, M.S. Dargusch, Grain refinement of wire arc additively manufactured titanium by the addition of silicon, J. Alloys Compd. 695 (2017) 2097–2103, doi:10.1016/j.jallcom.2016.11.049.

[12] B. Nagarajan, Z. Hu, X. Song, W. Zhai, J. Wei, Development of micro selective laser melting: the state of the art and future perspectives, Engineering 5 (2019) 702–720, doi:10.1016/j.eng.2019.07.002.

[13] A.G. Demir, Micro laser metal wire deposition for additive manufacturing of thin-walled structures, Opt. Lasers Eng. 100 (2018) 9–17, doi:10.1016/j.optlaseng.2017.07.003.

[14] S. Jhavar, C.P. Paul, N.K. Jain, Micro-plasma transferred arc additive manufacturing for die and mold surface remanufacturing, JOM 68 (2016) 1801–1809, doi:10.1007/s11837-016-1932-z.

[15] S. Jhavar, N.K. Jain, C.P. Paul, Development of micro-plasma transferred arc (μ-PTA) wire deposition process for additive layer manufacturing applications, J. Mater. Process. Technol. 214 (2014) 1102–1110, doi:10.1016/j.jmatprotec.2013.12.016.

[16] M. Terakubo, J. Oh, S. Kirihara, Y. Miyamoto, K. Matsuura, M. Kudoh, Freeform fabrication of titanium metal by 3D micro welding, Mater. Sci. Eng. A 402 (2005) 84–91, doi:10.1016/j.msea.2005.04.025.

[17] T.A. Rodrigues, V. Duarte, R.M. Miranda, T.G. Santos, J.P. Oliveira, Current status and perspectives on wire and arc additive manufacturing (WAAM), Materials 12 (2019) 1121 (Basel), doi:10.3390/ma12071121.

[18] V.R. Duarte, T.A. Rodrigues, N. Schell, R.M. Miranda, J.P. Oliveira, T.G. Santos, Hot forging wire and arc additive manufacturing (HF-WAAM), Addit. Manuf. 35 (2020) 101193, doi:10.1016/j.addma.2020.101193.

[19] S. Shin, M.S. Kim, S. Rhee, Prediction of weld porosity (pit) in gas metal arc welds, Int. J. Adv. Manuf. Technol. 104 (2019) 1109–1120, doi:10.1007/s00170-019-03853-5.